

# TUTDoR

## Optimal Trajectory Scheme for Robotic Welding Along Complex Joints Using a Hybrid Multi-Objective Genetic Algorithm.

Item Type	Article
Authors	Ogbemhe, John;Mpofu, Khumbulani;Tlale, Nkgatho
DOI	<a href="http://dx.doi.org/10.1109/ACCESS.2019.2950561">http://dx.doi.org/10.1109/ACCESS.2019.2950561</a>
Publisher	Institute of Electrical and Electronics Engineers
Rights	Attribution-NonCommercial-ShareAlike 4.0 International
Download date	2026-05-12 22:24:59
Item License	<a href="http://creativecommons.org/licenses/by-nc-sa/4.0/">http://creativecommons.org/licenses/by-nc-sa/4.0/</a>
Link to Item	<a href="https://hdl.handle.net/20.500.14519/1420">https://hdl.handle.net/20.500.14519/1420</a>

# Optimal Trajectory Scheme for Robotic Welding Along Complex Joints Using a Hybrid Multi-Objective Genetic Algorithm

JOHN OGBEMHE<sup>ID</sup>, KHUMBULANI MPOFU, AND NKGATHO TLALE

Department of Industrial Engineering, Tshwane University of Technology, Pretoria West 0183, South Africa

Corresponding author: John Ogbemhe (johnogbemhe@gmail.com)

**ABSTRACT** The problem of trajectory planning is relevant for the proper use of costly robotic systems to mitigate undesirable effects such as vibration and even wear on the mechanical structure of the system. The objective of this study is to design trajectories that are devoid of collision, velocity, acceleration, jerk and snap discontinuities so that the cycle time required to complete the process can be reduced. The trajectory design was constructed for all the six joints, using a 9<sup>th</sup> order Bezier curve to accommodate the ten boundary conditions required to satisfy the continuity constraints for joints displacement, velocity, acceleration, jerk and snap. The scheme combines the multi-objective genetic algorithm and the multi-objective goal attainment algorithm to solve the problem of total tracking error reduction during arc welding. The use of a hybrid multi-objective algorithm shows an improved average spread, average distance, number of iteration and computational time. Also, it can be concluded from the constraints studied, that the optimal path in terms of the robots dynamic constraints can achieve the expected tracking ability in terms of the optimal joint angles, velocities, acceleration, jerk, snap and torque.

**INDEX TERMS** Industrial robots, optimization, multi-objective genetic algorithm, trajectory planning, jerk, snap.

## I. INTRODUCTION

Industrial robots (IRs) have changed the face of manufacturing since their debut in the last decades, leading to tremendous advances in efficiency, capability and technology adoption. IRs have been applied to operations like material handling, arc-welding, painting, machining, assembly, material removal, part transfer and machine tending. In most of these IRs operations, the end-effector must move precisely in a smooth continuous routine along a specified trajectory. One of the most used applications of the industrial robot is robotic welding. Robotic welding is a term used to describe the use of an industrial robot to automate a welding process by performing the weld and handling part. Arc welding and resistance spot welding, employed in very high production applications, find huge aptness in robotic welding. Arc welding involves the use of a generated electric arc between an electrode and metal to heat and weld components together, permanently. As the torch is used to bond parts together, the shielding gas

The associate editor coordinating the review of this manuscript and approving it for publication was Ludovico Minati<sup>ID</sup>.



FIGURE 1. (a) Rail car body shell [1]; (b) Rail car bogie frame [2].

is used to prevent the sully of the molten weld pool to ensure a strong weld and to minimise post-weld clean up. For example, in railcar manufacturing, the welding process of the bogie frame and the body shell (see FIGURE 1) are usually made up of hundreds of complex welded joints components, which are known as tubular TYK. The schematic of the TYK joints is illustrated in FIGURE 2. The weldable parts constitute considerable size and complex geometry that needs to be joined along a curved path.

The welding process of the bogie frame is usually executed manually; it requires very high expertise by the operator and

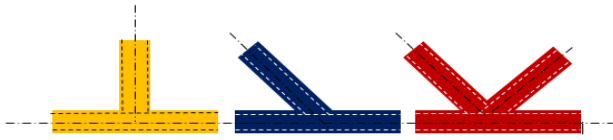


FIGURE 2. Common complex joints in various welding applications.

takes four days for two welders to implement. Even though commercially existing robotic welding systems are fortified using advanced welding technologies, automated welding solutions for this kind of complex joint without human intervention are near impossible due to the non-uniform and irregular geometries of the welding grooves.

Two essential methods exist for robot programming of robot task: On-line manual programming and Off-line programming have been applied to program robots for demanding tasks. On-line programming refers to physically teaching the robot the required trajectory, through interaction with the aid of a teach pendant or similar device; it has the benefit of being applied to the real-time situation since no testing is required. However, it has some setbacks including the possibility of collision; it is costly; the robot must be available; the production process has to be terminated [3]; and it requires technical expertise to understand the processes and programming skill of the robot. Off-line programming refers to graphical simulation frameworks that allow running manufacturing processes by using models of the real work-cells. The industrial robot is programmed into the simulator; hence, testing is required. The use of Off-line programming holds significant advantages. First, the cycle time can be determined beforehand. Second, no need to learn any of the robot programming languages but only the simulation language. Third, it is possible to build a work-cell around industrial robots by planning trajectories to avoid collisions. A robotic work-cell is used to denote robot, controller, and peripherals. It is still tricky for off-line programming to adequately represent the real world with maximum accuracy since programs may still need adjustment after they have been applied to the real robot [4].

The full benefits of industrial robots can only be achieved through proper trajectory planning. The problem of trajectory planning is relevant for appropriate use of the costly robotic systems to mitigate undesirable effects such as vibration and even wear on the mechanical structure of the system [5]–[7]. Rough and jerky motions cause increased wear and fluctuations in the robot by the excitation of resonance in the manipulator. Also, optimal trajectory planning plays a vital role in improving efficiency and reduction of the cycle time of the arc welding work-cell, even in the presence of constraints [5]. For example, a discontinuity in velocity leads to impulsive acceleration; a discontinuity in acceleration leads to impulsive jerk. Also, a discontinuity in jerk leads to impulsive snap. The snap, as used to denote the derivative of the jerk; is rarely considered as a constraint in trajectory planning of robotic work-cells. The significant contribution

of this paper is in solving the problem of discontinuity in jerk within the framework of the dynamic robot model during welding by the introduction of the Snap continuity constraint. The model uses a hybrid scheme that combines the global multi-objective genetic algorithm with the multi-objective goal attainment method; the hybrid scheme gives the advantages of both optimisation methods while counterweighing their disadvantages.

The rest of the paper is structured as follows. Section II discusses related works on the application of trajectory planning in robotic welding of complex joints. Section III and IV describe the trajectory design and formulation of the system, while section V describes the optimisation methodology used.

## II. RELATED WORK

For decades, trajectory planning for complex tasks in manufacturing work-cells has gained lots of attention from industrial robotics researchers. The objective of trajectory planning is to reduce cost angles, joint velocities, and joint acceleration function when subjected to joint jerks, torques and gripping force constraints by considering dynamics of the robot [8]. Trajectory planning is an integral part of robotic welding applications. The high operating speed requirement of robotic welding makes it imperative to design trajectories with suitable characteristics, to achieve meaningful output regarding quality and ease of performing the required motion. The capacity to generate trajectories with given characteristics, in terms of quality and ease of performing the required motion, especially, at high operating speeds required in many robotic applications is sacrosanct [9]. Robotic welding operations involve the end effector tracking a distinct trajectory, in three-dimensional space, as approximately, as attainable, while keeping the preferred velocity practically possible. Trajectory planning is not a trivial problem, bearing in mind the constraints imposed by the joint acceleration, end-effector velocity, and trajectory error. Disregarding these constraints gives rise to poor tracking performance: deviations of the end effector, overshoots, undue velocity fluctuations, rough and jerky motion. Several techniques have been used to design trajectory for robotic welding. For example, in [10], the authors used a trajectory generation methodology for a robotic Shielded metal arc welding (SMAW), whose execution time is a function of the melting rate of the electrode, and independent of the welding speed given by the welding parameters while keeping the electric arc length constant. The application establishes promising support for process design and manual welding training; however, the model did not factor jerk constraints. Efforts have been made by researches to solve the problem of jerk constraints. For example, Mattmüller and Gisler [11] designed a smooth and a near time trajectory to determine optimal jerk-constrained trajectories along three times differentiable paths in a non-perturbative manner. In [12], they designed a scheme which uses quintic and quartic polynomials to satisfy the continuity of the joints' positions, velocity, and acceleration; together

with the controllability of the acceleration at the end-path point. This was done to avoid the overshoot effect and system vibration and guarantee the stability of the robot motion. Chen and Li [13] employed acceleration and smooth jerk constraints to determine an optimal solution and transforming Kinematics constraints into the limitations on the optimal variables to reformulate the objective function in a matrix form; however, the model neglects the effect of robot dynamics. Also, Rubio, *et al.* [14] investigated the impact of torque, power, jerks, and energy consumed constraints on the design of minimum-time collision-free trajectories for industrial robots, whose algorithm works in a discrete configuration space, and inverse dynamics scheme. The scheme was analysed using cubic interpolation functions amid two adjacent configurations; improvement in the performance of the robot, by way of linking satisfactorily, the values of torque, power, jerk, and energy consumed was achieved. Freeman also follows a minimum jerk approach. In Freeman [15], the method of generating minimal jerk trajectories for redundant robots by using an algorithm based on the concept of a pseudo-spectral optimisation method was proposed. These models did not put the robot dynamic model into consideration.

Many recently proposed the use of off-line and virtual reality-based methods for robotic welding. Liu also made an effort to simulate a robotic arc welding process. In Liu, *et al.* [16], the authors introduced a simulation system for arc welding design and task planning that converts the design features (including connection and constraints) of the workpiece to the machining features (including seam axis, normal, start and endpoints) of the seams, and then directs the robot to perform the welding task.

Furthermore, optimisation models have been applied to plan paths for welding robots. Chen also proposed a method for solving partitioning of the path during welding. In [17], they defined welding paths of tube-sphere intersection based on the established J-groove joint robot; the point inversion module using particle swarm optimisation (PSO) was proposed to address the difficulty of the partitioning of the path required in the welding process.

New methodologies have been proposed for solving the trajectory problem in industrial robotics. [18], designed a real-time path smoothing method for DELTA parallel using a 5<sup>th</sup> order Bezier to blend the adjacent linear segments. [19], proposed a robot path planning method in which the welding task is divided into multiple intervals. The trajectory is modelled as both a line and arc interpolation transition, to complete the welding task from both joint and Cartesian coordinate space planning. Reference [20] achieved a significantly shorter cycle time with stable motion performance of velocities, accelerations, and jerk using a methodology based on the 3-4-5 polynomial motion and Quintic Pythagorean-Hodograph (PH) curves. Time-optimal trajectory planning in real-time, using pseudoinverse-based, path-constrained for a kinematically redundant robot under torque and velocity constraints robot has been reported [21], [22].

Unlike the methods as mentioned above, we designed a trajectory for the six joints, using a nonic Bezier curve to accommodate the ten boundary conditions required to satisfy the continuity constraints for joints displacement, velocity, acceleration, jerk and snap. The control point at the initial and final condition during welding is premised on the assumption that the robot is at rest initially, and comes to a full stop at the end of the trajectory. The algorithm developed uses a hybrid scheme that combines the global multi-objective genetic algorithm with the multi-objective goal attainment method; the hybrid scheme gives the advantages of both optimisation methods while counterweighing their disadvantages.

### III. TRAJECTORY DESIGN

Trajectory planning and generation of motion of the arc-welding gun are vital in the welding of complex joints found in railcar manufacturing. The task requires that the arc-welding gun pass a warped curve, like those experienced at the seam of the warped surfaces found in the underframe of a rail wagon and the bogie frame. The use of a six-degree of freedom robot ensures the welding torch can reach an arbitrary posture and finish the welding task.

#### A. PATH ORIENTATION USING EULER ANGLES

To provide orientation information during arc welding, the authors employed Euler angles. Euler angles are more humanly comprehensible and ideal for decomposing rotations into degrees of freedom based on the joint kinematics. The orientation is defined using *ZYX* convention and within the Cartesian coordinates system. The roll, pitch and yaw vectors defines the coordinate frame and describes the orientation of the industrial robot joints (see Appendix FIGURE 13). Digital Enterprise Lean Manufacturing Interactive Application (DELMIA), and Catia 3D software uses the *ZYX* convention that is also good for the alignment of notation and convention. See the Appendix Section for the Euler angles equations (26)-(28), defined by using the *ZYX* convention. Also, to find a robust, optimal solution during arc welding, a nonic Bezier curve is derived to address the limitation of using a higher-order polynomial caused by numerical problems due to bad conditioning. The objective of the optimisation problem is to carry out the welding task with minimum movement of the joint angles along with the weld points, in the presence of both kinematic and dynamic constraints.

#### B. KINEMATIC AND DYNAMIC MODEL OF THE ROBOT

The dynamic equation of the industrial robot is derived using Lagrangian, which is the difference between the kinetic energy and its potential energy. The dynamic equation of the systems in terms of the Euler-Lagrangian method and incorporating friction terms and path constraints are summarised in (1).

$$Z_{\min} = \sum_{j=1}^N (M(\theta) \ddot{\theta} + H(\theta, \dot{\theta}) + G(\theta) + \tau_{fric}(\theta, \dot{\theta}))$$

s.t. constraints

$$\begin{aligned}
 |\theta_j| &\leq \theta_j^{\max} = \text{displacement} \\
 |\dot{\theta}_j| &\leq \dot{\theta}_j^{\max} = \text{velocity} \\
 |\ddot{\theta}_j| &\leq \ddot{\theta}_j^{\max} = \text{acceleration} \\
 |\ddot{\theta}_j| &\leq \ddot{\theta}_j^{\max} = \text{jerk} \\
 |\ddot{\theta}_j| &\leq \ddot{\theta}_j^{\max} = \text{snap}
 \end{aligned} \tag{1}$$

where,  $Z_{\min}$  is the objective function depicting the joint torque vector  $\tau$ ,  $M$  is the joint space symmetric inertia matrix,  $H$  is the vector of centrifugal and Coriolis forces,  $G$  is the gravity force vector,  $\tau_{fric}$  is the frictional forces and  $\theta, \dot{\theta}, \ddot{\theta}$  are the joint angles velocity and acceleration vectors. The descriptions of all the variables in (1) are reported in Table 1.

TABLE 1. Description of variables of the robot dynamic equations.

Vector/Matrix	Description
$\{\tau\}$	The vector of applied joint torques
$[M(\theta)]$	$N \times N$ Mass matrix; symmetric and positive definite
$\{H(\theta, \dot{\theta})\}$	$N \times 1$ The vector of Coriolis and centripetal terms
$\{\tau_{fric}(\theta, \dot{\theta})\}$	$N \times 1$ The vector of friction torques
$G(\theta)$	$N \times 1$ The vector of gravity terms
$\{\theta\}, \{\dot{\theta}\}, \{\ddot{\theta}\}$	$N \times 1$ Joints angles, rates, and acceleration vectors

C. WELDING SYSTEM

The robotic welding system is made up of sub-systems: arc welding industrial robot, workpiece positioners/fixtures, power source, wire feeder, welding gun or torch, torch cleaner, risers, control systems, tool centre point (TCP) calibration unit, and so forth. The industrial robot whose dynamic model is described in (1) and TABLE 1 is a fundamental sub-system of the welding systems, and it influences the quality of the weld. The Denavit Hartenberg (DH) approach is applied to define the industrial robot coordinate system. For ease of analysis of the kinematic equation, the last three joints are set as a reference point on the wrist, and the first three joint axes intersect at one point, the reference point in the wrist.

The framework described in FIGURE 3 is used to build the robotic work cell. Tags, as used in this section, denote coordinate points used to carry welding operations; they are constructed to guarantee a consistent path for the robot. The path is re-ordered after it is created or in the middle of the process. The created tags are grouped in a tag list where it is used to define and assign a task to the industrial robot. The created tags are placed around the points to be welded followed by the creation of a task that fuses the tags points across the product. See FIGURE 4 for a screenshot on the use of the Delmia robotics to manipulate the Process Product Resource (PPR) and design the work cell, containing robot, riser, Bogie and the positioner. FIGURE 5 shows the work-cell simulation of

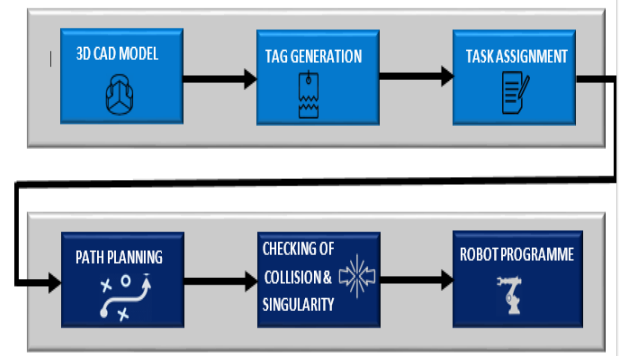


FIGURE 3. Framework adopted for off-line programming.

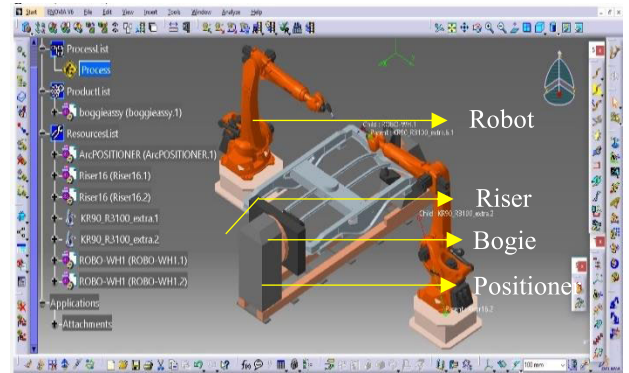


FIGURE 4. Screenshot of designed arc welding work cell for KUKA KR90.

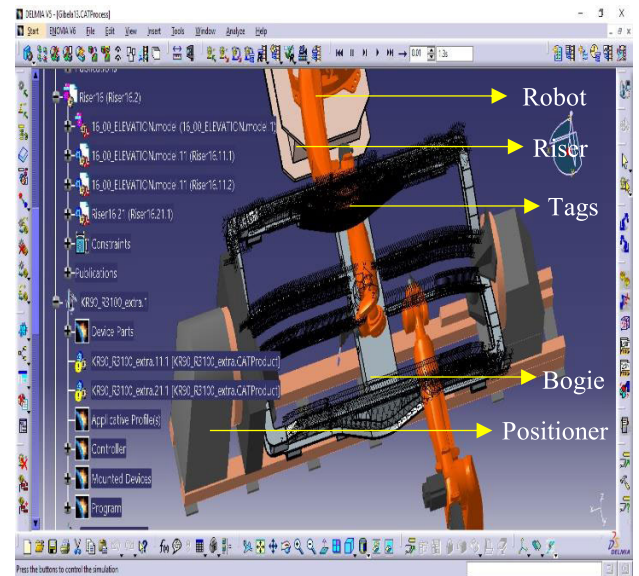


FIGURE 5. Work cell simulation Arc welding.

the arc welding. The simulation results provide inputs used to determine the control points of the Bezier curve for  $t \in [0, 1]$ . The riser provides a platform for mounting the industrial robot. Tags are used to define points on the bogie frame to be welded, and the positioner grips the bogie during arc welding.

### IV. TRAJECTORY FORMULATION

The trajectory was constructed for all the six joints by using the nonic Bezier curve, and the Bezier function  $\theta_i(t)$  is defined on the interval  $[t_i, t_{i+1}]$ . The continuity of Displacement, Velocity, Acceleration, Jerk and Snap (DVAJS) is assumed all through the formulation. Ten boundary conditions are required to impose these continuity constraints. It is convenient to use the polynomial function of a degree  $n$  in normalised form, for example as

$$\theta_N(t) = c_0 + c_1t + c_2t^2 + c_3t^3 + c_4t^4 + \dots + c_nt^n \quad (2)$$

In order to determine the parameters  $c_n$  in (2), the mathematical relationship in (3) is defined as

$$\mathbf{Dc} = \mathbf{b}, \quad (3)$$

where  $\mathbf{c} = [c_0, c_1, c_2, c_3, \dots, c_n]^T$ . The vector  $\mathbf{b}$ , containing the boundary conditions of displacement, velocity, acceleration, jerk and snap will take the form in (4).

$$\mathbf{b} = [q_0, v_0, a_0, j_0, s_0, q_1, v_1, a_1, j_1, s_1]^T \quad (4)$$

Lastly, the coefficient matrix  $\mathbf{D}$  is defined by imposing the boundary conditions on (5). The parameters  $\mathbf{c}$  are determined using

$$\mathbf{c} = \mathbf{D}^{-1}\mathbf{b} \quad (5)$$

As the degree of the polynomial increases, the computation of  $\mathbf{D}^{-1}$  may give numerical issues. This research uses the Bezier form of polynomials to address the shortcoming of the conventional polynomial scheme. The Bezier polynomial is expressed in the form of

$$\theta_N(t) = \sum_{i=0}^n \binom{n}{i} t^i (1-t)^{n-1} p_i, \quad 0 \leq t \leq 1 \quad (6)$$

where  $\binom{n}{i}$  is the binomial coefficient defined as  $\binom{n}{i} = \frac{n!}{i!(n-i)!}$ ;  $t$  is the parameter that influences the distribution of the interpolation points;  $\binom{n}{i} t^i (1-t)^{n-1}$  are the Bernstein polynomials and  $p_i$  are known as the control points. The relationship between the control points  $p_i$  and coefficients  $c_i$  is shown in (7) [23].

$$c_j = \frac{n!}{(n-j)!} \sum_{i=0}^j \frac{(-1)^{i+j}}{i!(j-i)!} p_i, \quad j = 0, 1, \dots, n. \quad (7)$$

Similarly, the control points  $p_i$  are calculated by imposing the boundary conditions on (6) at both the initial and final points.

#### A. PATH MODELLING USING NONIC BEZIER CURVE

Applying the generalised Bezier polynomial function in (6) yields the expression in (8)

$$\begin{aligned} \theta_N(t) = & \left( -t^9 + 9t^8 - 36t^7 + 84t^6 - 126t^5 \right) p_0 \\ & + \left( +126t^4 - 84t^3 + 36t^2 - 9t + 1 \right) p_1 \\ & + \left( 9t^9 - 72t^8 + 252t^7 - 504t^6 + 630t^5 \right) p_1 \\ & + \left( -504t^4 + 252t^3 - 72t^2 + 9t \right) p_4 \end{aligned}$$

$$\begin{aligned} & + \left( -36t^9 + 252t^8 - 756t^7 + 1260t^6 \right) p_2 \\ & + \left( -1260t^5 + 756t^4 - 252t^3 + 36t^2 \right) p_2 \\ & + \left( 84t^9 - 504t^8 + 1260t^7 - 1680t^6 \right) p_3 \\ & + \left( +1260t^5 - 504t^4 + 84t^3 \right) p_3 \\ & + \left( -126t^9 + 630t^8 - 1260t^7 + 1260t^6 \right. \\ & \left. - 630t^5 + 126t^4 \right) p_4 \\ & + \left( 126t^9 - 504t^8 + 756t^7 - 504t^6 + 126t^5 \right) p_5 \\ & + \left( -84t^9 + 252t^8 - 252t^7 + 84t^6 \right) p_6 \\ & + \left( 36t^7(1-t)^2 \right) p_7 + \left( 9t^8(1-t) \right) p_8 + \left( t^9 \right) p_9 \end{aligned} \quad (8)$$

Differentiating the expression in (8) yields the acceleration continuity expression in (9).

$$\begin{aligned} \dot{\theta}_N(t) = & \left( -9t^8 + 72t^7 - 252t^6 + 504t^5 \right) p_0 \\ & + \left( -630t^4 + 504t^3 - 252t^2 + 72t - 9 \right) p_0 \\ & + \left( 81t^8 - 576t^7 + 1764t^6 - 3024t^5 + \right. \\ & \left. 3150t^4 - 2016t^3 + 756t^2 - 144t + 9 \right) p_1 \\ & + \left( -324t^8 + 2016t^7 - 5292t^6 + 7560t^5 \right) p_2 \\ & + \left( -6300t^4 + 3024t^3 - 756t^2 + 72t \right) p_2 \\ & + \left( 756t^8 - 4032t^7 + 8820t^6 - 10080t^5 \right) p_3 \\ & + \left( +6300t^4 - 2016t^3 + 252t^2 \right) p_3 \\ & + \left( -1134t^8 + 5040t^7 - 8820t^6 + 7560t^5 \right. \\ & \left. - 3150t^4 + 504t^3 \right) p_4 \\ & + \left( 1134t^8 - 4032t^7 + 5292t^6 - 3024t^5 + 630t^4 \right) p_5 \\ & + \left( -756t^8 + 2016t^7 - 1764t^6 + 504t^5 \right) p_6 \\ & + \left( 324t^8 - 576t^7 + 252t^6 \right) p_7 \\ & + \left( -81t^8 + 72t^7 \right) p_8 + \left( 9t^8 \right) p_9 \end{aligned} \quad (9)$$

Differentiating the expression in (9) yields the acceleration continuity expression in (10).

$$\begin{aligned} \ddot{\theta}_N(t) = & \left( -72t^7 + 504t^6 - 1512t^5 + 2520t^4 - \right) p_0 \\ & \left( 2520t^3 + 1512t^2 - 504t + 72 \right) p_0 \\ & + \left( 648t^7 - 4032t^6 + 10584t^5 - 15120t^4 \right) p_1 \\ & + \left( +12600t^3 - 6048t^2 + 1512t - 144 \right) p_1 \\ & + \left( -2592t^7 + 14112t^6 - 31752t^5 + 37800t^4 \right) p_2 \\ & + \left( -25200t^3 + 9072t^2 - 1512t + 72 \right) p_2 \\ & + \left( 6048t^7 - 28224t^6 + 52920t^5 - \right) p_3 \\ & \left( 50400t^4 + 25200t^3 - 6048t^2 + 504t \right) p_3 \\ & + \left( -9072t^7 + 35280t^6 - 52920t^5 \right) p_4 \\ & + \left( +37800t^4 - 12600t^3 + 1512t^2 \right) p_4 \\ & + \left( 9072t^7 - 28224t^6 + 31752t^5 \right) p_5 \\ & + \left( -15120t^4 + 2520t^3 \right) p_5 \\ & + \left( -6048t^7 + 14112t^6 \right) p_6 \\ & + \left( -10584t^5 + 2520t^4 \right) p_6 \end{aligned}$$

$$\begin{aligned}
 &+ (2592t^7 - 4032t^6 + 1512t^5) p_7 \\
 &+ (-648t^7 + 504t^6) p_8 + (72t^7) p_9 \quad (10)
 \end{aligned}$$

Differentiating the expression in (10) yields the jerk continuity expression in (11).

$$\begin{aligned}
 &\ddot{\theta}_N(t) \\
 &= \begin{pmatrix} -504t^6 + 3024t^5 - 7560t^4 + 10080t^3 \\ -7560t^2 + 3024t - 504 \end{pmatrix} p_0 \\
 &+ \begin{pmatrix} 4536t^6 - 24192t^5 + 52920t^4 - 60480t^3 \\ +37800t^2 - 12096t + 1512 \end{pmatrix} p_1 \\
 &+ \begin{pmatrix} -18144t^6 + 84672t^5 - 158760t^4 + \\ 151200t^3 - 75600t^2 + 18144t - 1512 \end{pmatrix} p_2 \\
 &+ \begin{pmatrix} 42336t^6 - 169344t^5 + 264600t^4 \\ -201600t^3 + 75600t^2 - 12096t + 504 \end{pmatrix} p_3 \\
 &+ \begin{pmatrix} -63504t^6 + 211680t^5 - 264600t^4 \\ +151200t^3 - 37800t^2 + 3024t \end{pmatrix} p_4 \\
 &+ \begin{pmatrix} 63504t^6 - 169344t^5 + 158760t^4 \\ -60480t^3 + 7560t^2 \end{pmatrix} p_5 \\
 &+ \begin{pmatrix} -42336t^6 + 84672t^5 - 52920t^4 + 10080t^3 \end{pmatrix} p_6 \\
 &+ \begin{pmatrix} 18144t^6 - 24192t^5 + 7560t^4 \end{pmatrix} p_7 \\
 &+ \begin{pmatrix} -4536t^6 + 3024t^5 \end{pmatrix} p_8 + \begin{pmatrix} 504t^6 \end{pmatrix} p_9 \quad (11)
 \end{aligned}$$

Differentiating the expression in (11) yields the snap continuity expression in (12).

$$\begin{aligned}
 &\dddot{\theta}_N(t) = \begin{pmatrix} -3024t^5 + 15120t^4 - 30240t^3 \\ +30240t^2 - 15120t + 3024 \end{pmatrix} p_0 \\
 &+ \begin{pmatrix} 27216t^5 - 120960t^4 + 211680t^3 \\ -181440t^2 + 75600t - 12096 \end{pmatrix} p_1 \\
 &+ \begin{pmatrix} -108864t^5 + 423360t^4 - 635040t^3 \\ +453600t^2 - 151200t + 18144 \end{pmatrix} p_2 \\
 &+ \begin{pmatrix} 254016t^5 - 846720t^4 + 1058400t^3 \\ -604800t^2 + 151200t - 12096 \end{pmatrix} p_3 \\
 &+ \begin{pmatrix} -381024t^5 + 1058400t^4 - 1058400t^3 \\ +453600t^2 - 75600t + 3024 \end{pmatrix} p_4 \\
 &+ \begin{pmatrix} 381024t^5 - 846720t^4 + 635040t^3 \\ -181440t^2 + 15120t \end{pmatrix} p_5 \\
 &+ \begin{pmatrix} -254016t^5 + 423360t^4 \\ -211680t^3 + 30240t^2 \end{pmatrix} p_6 \\
 &+ \begin{pmatrix} 108864t^5 - 120960t^4 + 30240t^3 \end{pmatrix} p_7 \\
 &+ \begin{pmatrix} -27216t^5 + 15120t^4 \end{pmatrix} p_8 + \begin{pmatrix} 3024t^5 \end{pmatrix} p_9 \quad (12)
 \end{aligned}$$

**B. DETERMINATION OF THE CONTROL POINT AT INITIAL AND FINAL CONDITION**

The parameters  $p_i$  in (6) are computed by first imposing the boundary conditions on  $\theta_N(t)$ , by using (8)-(12). The

resulting boundary condition is provided in (13)-(14).

$$\begin{aligned}
 &\theta_N(0) = q_0; \quad \dot{\theta}_N(0) = v_0; \quad \ddot{\theta}_N(0) = a_0; \\
 &\ddot{\theta}_N(0) = j_0; \quad \dddot{\theta}_N(0) = s_0. \quad (13)
 \end{aligned}$$

$$\begin{aligned}
 &\theta_N(1) = q_1; \quad \dot{\theta}_N(1) = v_1; \quad \ddot{\theta}_N(1) = a_1; \\
 &\ddot{\theta}_N(1) = j_1; \quad \dddot{\theta}_N(1) = s_1. \quad (14)
 \end{aligned}$$

Re-writing (3) in terms of the control points at  $t = 0$  yields (15).

$$\mathbf{D}_0 \mathbf{p}_0 = \mathbf{b}_0, \quad (15)$$

with

$$\begin{aligned}
 \mathbf{D}_0 &= \begin{bmatrix} 1 & 0 & 0 & 0 & 0 & 0 & 0 & 0 & 0 & 0 \\ -1 & 1 & 0 & 0 & 0 & 0 & 0 & 0 & 0 & 0 \\ 1 & -2 & 1 & 0 & 0 & 0 & 0 & 0 & 0 & 0 \\ -1 & 3 & -3 & 1 & 0 & 0 & 0 & 0 & 0 & 0 \\ -1 & -4 & 6 & -4 & 1 & 0 & 0 & 0 & 0 & 0 \end{bmatrix}; \\
 \mathbf{b}_0 &= \begin{bmatrix} q_0 \\ v_0 \\ n \\ a_0 \\ \frac{n(n-1)}{j_0} \\ \frac{n(n-1)(n-2)}{s_0} \\ \frac{n(n-1)(n-2)(n-3)}{s_0} \end{bmatrix} \quad (16)
 \end{aligned}$$

Similarly, the control points at  $t = 1$  yields (17).

$$\mathbf{D}_1 \mathbf{p}_1 = \mathbf{b}_1, \quad (17)$$

with

$$\begin{aligned}
 \mathbf{D}_1 &= \begin{bmatrix} 1 & 0 & 0 & 0 & 0 & 0 & 0 & 0 & 0 & 0 \\ -1 & 1 & 0 & 0 & 0 & 0 & 0 & 0 & 0 & 0 \\ 1 & -2 & 1 & 0 & 0 & 0 & 0 & 0 & 0 & 0 \\ -1 & 3 & -3 & 1 & 0 & 0 & 0 & 0 & 0 & 0 \\ -1 & -4 & 6 & -4 & 1 & 0 & 0 & 0 & 0 & 0 \end{bmatrix}; \\
 \mathbf{b}_1 &= \begin{bmatrix} q_1 \\ v_1 \\ n \\ a_1 \\ \frac{n(n-1)}{j_1} \\ \frac{n(n-1)(n-2)}{s_1} \\ \frac{n(n-1)(n-2)(n-3)}{s_1} \end{bmatrix} \quad (18)
 \end{aligned}$$

The control points for both the initial and final condition are calculated by using the expression  $\mathbf{p}_0 = \mathbf{D}_0^{-1} \mathbf{b}_0$  and  $\mathbf{p}_1 = \mathbf{D}_1^{-1} \mathbf{b}_1$ , derived from (16) and (18). The parameters in  $\mathbf{b}_0$  and  $\mathbf{b}_1$  are obtained from the result of the robotic off-line simulation.

These control points values are substituted in (8)-(12) to arrive at the much-needed continuity condition (see TABLE 3), on the assumption that the robot is at rest initially, and comes to full rest at the end of the trajectory.

TABLE 2 shows the control points used at the initial and final condition and TABLE 3 gives the velocities, acceleration, jerk, and snap constraints for KR90-R3100-Extra

TABLE 2. Control points at initial and final points.

Joints	Control points at t=0					Control points at t=1				
	$P_0$	$P_1$	$P_2$	$P_3$	$P_4$	$P_5$	$P_6$	$P_7$	$P_8$	$P_9$
1	-1102.40	-735.49	-367.90	0.5530	370	-1102.40	-735.49	-367.90	0.5530	370
2	-504.68	-336.96	-168.69	0.2450	170	-504.68	-336.96	-168.69	0.2450	170
3	-831.06	-554.97	-277.85	0.4138	280	-831.06	-554.97	-277.85	0.4138	280
4	-2082200	-1389.90	-695.54	1.0302	700	-2082200	-1389.9	-695.54	1.0302	700
5	-794.03	-531.28	-266.60	0.3724	270	-794.03	-531.28	-266.60	0.3724	270
6	-2077.20	-1387.20	-694.56	1.0316	700	-2077.20	-1387.20	-694.56	1.0316	700

TABLE 3. Kinematic constraint for KR90-extra robot.

Kinematic Constraint	Joint1	Joint 2	Joint 3	Joint 4	Joint 5	Joint 6
$\dot{\theta}_{max}$ (deg s <sup>-1</sup> ) - Velocity Continuity	105	101	107	292	258	284
$\ddot{\theta}_{max}$ (deg s <sup>-2</sup> ) - Acceleration Continuity	52	50	80	136	178	206
$\dddot{\theta}_{max}$ (deg s <sup>-3</sup> ) - Jerk Continuity	75	75	82	100	190	200
$\ddot{\theta}_{max}$ (deg s <sup>-4</sup> ) - Snap Continuity	100	100	95	90	105	150

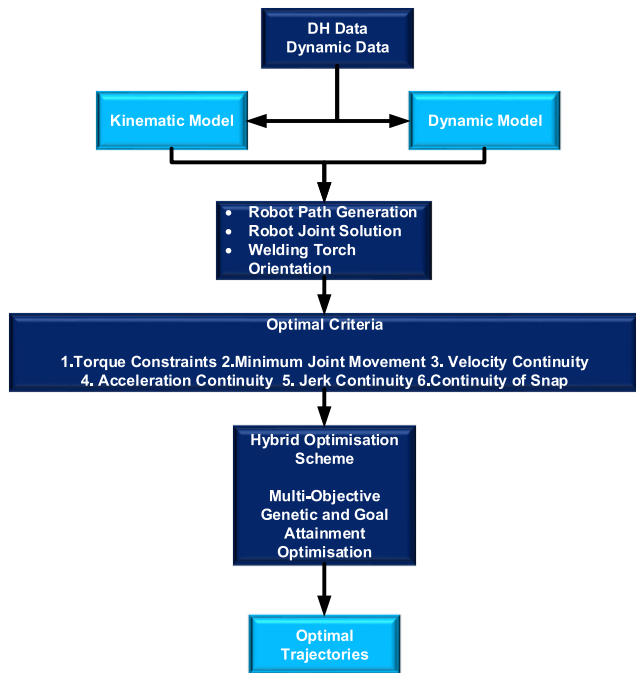


FIGURE 6. Optimisation approach.

robot [24]; the maximum permissible torque for the robot is 35000Nm.

### V. OPTIMISATION APPROACH

FIGURE 6 presents an overall analysis of the algorithm and code development that incorporates both the dynamic model shown in (1) and the constraints formulated in Section IV. Evolutionary Algorithms (EA) are suitable for solving Multi-Objective Problems (MOPs), thanks to their ability to provide the decision-makers with a set of trade-off solutions in a single run and also for their insensitivity to the geometric features of the objective space. A MOP consists of minimising

or maximising an objective function vector under constraints. The generalised robotic model in the form of MOPs is as follows:

$$\begin{cases}
 \text{Min} \tau(x) = [\tau_1(x), \tau_2(x), \dots, \tau_N(x)]^T \\
 \gamma_j(x) \geq 0 & j = 1, \dots, Q \\
 h_k(x) = 0 & k = 1, \dots, R \\
 x_i^L \leq x_i \leq x_i^U & i = 1, \dots, n
 \end{cases} \quad (19)$$

where  $N$  is the number of the objective functions,  $Q$  is the number of the inequality constraints,  $R$  is the number of equality constraints,  $x_i^L$  and  $x_i^U$  are the lower and upper bounds. The solution  $x_i$  satisfying the constraints  $Q + R$  is feasible, and the set of all feasible solutions defines the feasible search space denoted by  $\Omega$  in (19). A trade-off solution is achieved during the determination of the MOP; this solution is known as the Pareto optimal solutions.

An optimisation is a process of manipulating inputs into a model to find the minimum or maximum result; this process will be referred to here as the evaluation function. An optimisation algorithm finds the optimum solution among so many local minima. It is of interest to know that some optimisation schemes are better equipped for finding a local minimum rather than finding a global minimum. The genetic algorithm is a search algorithm founded on the mechanism of natural genetics and natural selections. GA, a branch of the evolutionary, computation techniques applies the physical survival of the fittest with genetic operators abstracted from nature to form a very robust search mechanism that has become popular with optimal robotics problems [25]. The use of GA involves a pool of possible solution space to the evaluation function; undergoing mutation, creating new offspring and the process repeated in a series of generations. The use of GA as a non-derivative optimisation scheme has numerous advantages, such as:

1. More efficient than the traditional methods of optimisation,
2. Excellent parallel computing capabilities for both continuous, discrete function and multi-objective problems,
3. GA finds good application for large search space, and with lots of parameters.

However, the use of GA comes with its challenges including inconsistency of search space solutions; its time-consuming nature and difficulty dealing with equality constraints. To address this setback, this paper adopts the Multi-objective GA and goal attainment algorithm as a hybrid optimisation scheme. This hybrid scheme optimises the joint angles so that the end-effector tracks the prescribed trajectory smoothly and accurately in the presence of velocity, jerk, and snap continuity.

### A. OPTIMISATION PROBLEMS AND THE DESIGN VARIABLES CONSTRAINTS

The mathematical statement of the optimisation problem for the robots, regarding dynamics, is as stated in (1); subject to joints constraints in (20), velocity constraints in (21), acceleration constraints in (22), jerk constraints in (23), and snap constraints in (24) respectively.

$$\begin{aligned} x_1 \leq \theta_1 = 185^0; -x_1 \leq \theta_1 = 185; x_2 \leq \theta_2 = -5^0; \\ -x_2 \leq \theta_2 = -140^0; x_3 \leq \theta_3 = 155^0; \\ -x_3 \leq \theta_3 = 120^0; x_4 \leq \theta_4 = 350^0; -x_4 \leq \theta_4 = 350^0; \\ x_5 \leq \theta_5 = 125^0; -x_5 \leq \theta_5 = 125^0; x_6 \leq \theta_6 = 350^0; \\ -x_6 \leq \theta_6 = 350^0 \end{aligned} \quad (20)$$

$$\begin{aligned} x_7 \leq \dot{\theta}_1 = 105 \text{ deg } s^{-1}; x_8 \leq \dot{\theta}_2 = 101 \text{ deg } s^{-1}; \\ x_9 \leq \dot{\theta}_3 = 107 \text{ deg } s^{-1}; x_{10} \leq \dot{\theta}_4 = 292 \text{ deg } s^{-1}; \\ x_{11} \leq \dot{\theta}_5 = 258 \text{ deg } s^{-1}; x_{12} \leq \dot{\theta}_6 = 284 \text{ deg } s^{-1} \end{aligned} \quad (21)$$

$$\begin{aligned} x_{13} \leq \ddot{\theta}_1 = 52 \text{ deg } s^{-2}; x_{14} \leq \ddot{\theta}_2 = 50 \text{ deg } s^{-2}; \\ x_{15} \leq \ddot{\theta}_3 = 80 \text{ deg } s^{-2}; x_{16} \leq \ddot{\theta}_4 = 136 \text{ deg } s^{-2}; \\ x_{17} \leq \ddot{\theta}_5 = 178 \text{ deg } s^{-2}; x_{18} \leq \ddot{\theta}_6 = 206 \text{ deg } s^{-2} \end{aligned} \quad (22)$$

$$\begin{aligned} x_{19} \leq \dddot{\theta}_1 = 75 \text{ deg } s^{-3}; x_{20} \leq \dddot{\theta}_2 = 75 \text{ deg } s^{-3}; \\ x_{21} \leq \dddot{\theta}_3 = 82 \text{ deg } s^{-3}; x_{22} \leq \dddot{\theta}_4 = 100 \text{ deg } s^{-3}; \\ x_{23} \leq \dddot{\theta}_5 = 190 \text{ deg } s^{-3}; x_{24} \leq \dddot{\theta}_6 = 200 \text{ deg } s^{-3} \end{aligned} \quad (23)$$

$$\begin{aligned} x_{25} \leq \overset{\cdot\cdot\cdot}{\theta}_1 = 100 \text{ deg } s^{-4}; x_{26} \leq \overset{\cdot\cdot\cdot}{\theta}_2 = 100 \text{ deg } s^{-4}; \\ x_{27} \leq \overset{\cdot\cdot\cdot}{\theta}_3 = 95 \text{ deg } s^{-4}; x_{28} \leq \overset{\cdot\cdot\cdot}{\theta}_4 = 90 \text{ deg } s^{-4}; \\ x_{29} \leq \overset{\cdot\cdot\cdot}{\theta}_5 = 105 \text{ deg } s^{-4}; x_{30} \leq \overset{\cdot\cdot\cdot}{\theta}_6 = 150 \text{ deg } s^{-4} \end{aligned} \quad (24)$$

Finally, the dynamic constraint is expressed in (25).

$$\tau_i \leq \tau_{i \max} \quad (25)$$

The expression  $\tau_i$  and  $\tau_{i \max}$  is the torque and the maximum torque of the  $i_{th}$  link, respectively. The design and optimisation techniques involve the search and identification of the best configuration that minimises the joints angle movements. These techniques guarantee that the end-effector tracks the prescribed arc weld trajectory smoothly and accurately in the presence of dynamic and kinematic constraints,

thereby minimising the torque requirement of the robot. The trajectory optimisation constraints equations, described in (20)-(25) were employed to run the optimisation iterations. Figure 3 shows the flow chart of the optimal trajectory planning using the hybrid, multi-objective goal attainment optimisation scheme.

### B. HYBRID OPTIMISATION PARAMETERS

The hybrid optimisation scheme, which integrates the benefits of the multi-objective genetic algorithm and the multi-objective goal attainment algorithm is proposed in this section. The hybrid optimisation uses adaptive parameters to regulate the probabilities of the mutation, cross-over and population size operators until the maximum solution space is achieved. The crossover probability is used to describe how repeatedly the crossover can be performed, for example, if there is no crossover, the offspring are the same copy as that of the parents, and if there is a crossover, the offspring is made from parts of the parent's chromosome. A cross over the probability of 0%, indicates a new generation is produced from the exact copies; while a 100% crossover probability indicates that all offspring are produced by crossover. The mutation is a critical parameter that stops the GA from being function at a score range of 0 and a maximum number of the individual at 7 see FIGURE 8. The mutation is a caught up in local minima. The mutation probability is used to describe how parts of the chromosome are mutated. A mutation probability of 100% indicates that the whole chromosome is changed while a 0% mutation probability indicates that nothing is changed. The optimisation parameters are as shown in TABLE 4.

The relationship between the average speeds of the generational chromosomes gives the average spread of 0.0373923, as shown in FIGURE 8. The average distance between the individuals 500 generation is described in FIGURE 8. The selection function by using tournament, in terms of the number of children and its chromosomes show the number of children as seven in a population size of 200; see FIGURE 8. The score histogram gives an optimal multi-objective evaluation.

## VI. RESULT AND DISCUSSION OF THE OPTIMISATION SIMULATION ANALYSIS

The fundamental assumption made in this section is that the robot is at rest initially, and comes to a full stop at the end of the trajectory. The ensuing dynamic equation modelled as a function of (DVAJS) constraints were optimised using the multi-objective genetic and multi-objective goal attainment algorithm of the global optimisation toolbox in MATLAB 2019a. The effects of the defined constraints on the optimised Snap is reported and discussed in this section. However, the result of the defined constrained on displacement, velocity, jerk and torque are shown in the Appendix section. The coefficient of determination, known as R-SQUARE, gives the goodness of fit of the observed data.

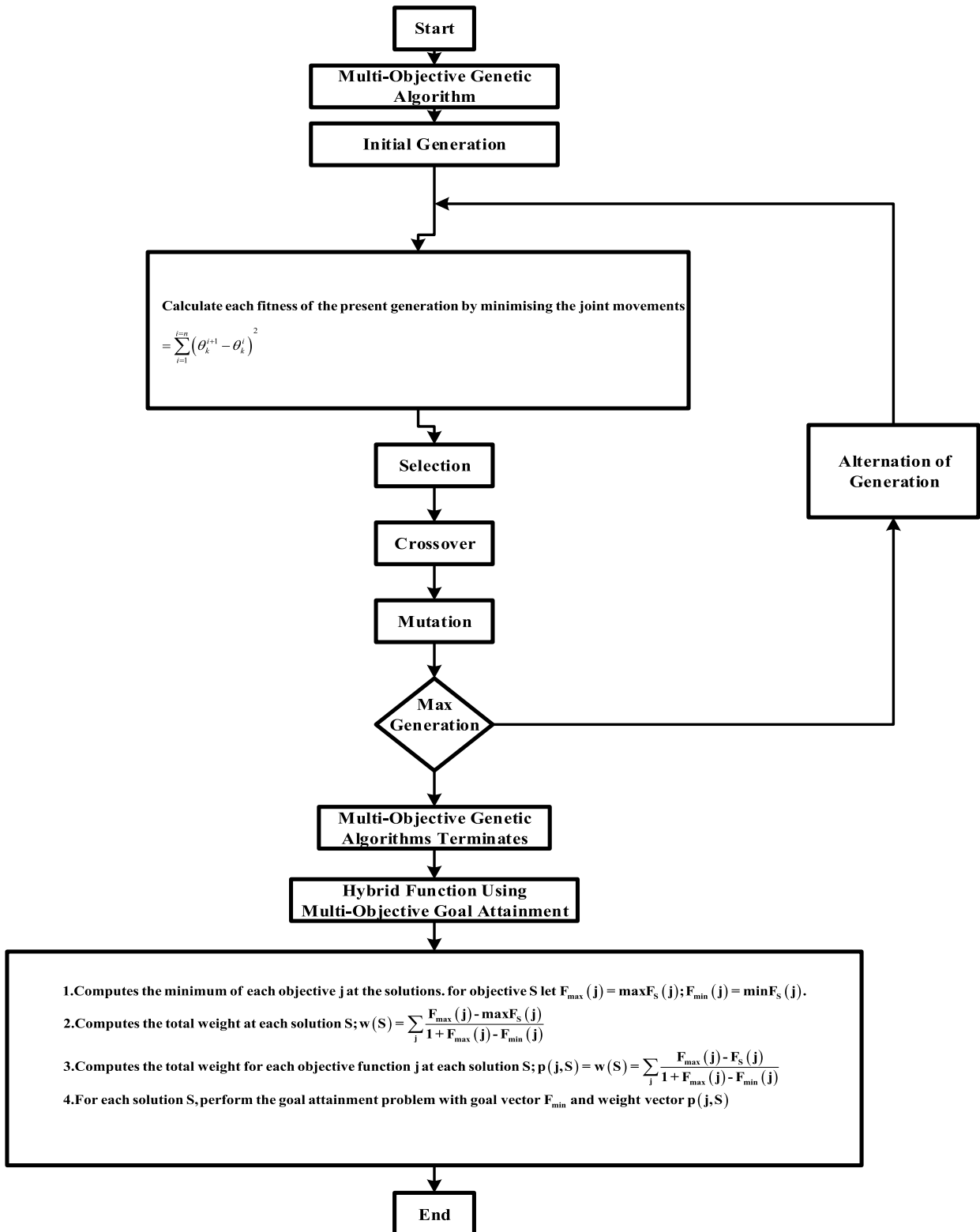


FIGURE 7. Flow chart of optimal trajectory planning using hybrid multi-objective and goal attainment optimisation scheme.

**A. EFFECT OF THE DEFINED CONSTRAINTS ON THE OPTIMISED JOINT DVAS**

To validate the effect of the defined constraints on the joint snap, the classical Multi-Objective Genetic Algorithm

(MOGA) and the Hybrid Multi-Objective Genetic Algorithm (HMOGA) optimisation were used. The coefficient of determination, known as R-SQUARE, gives the goodness of fit of the observed data. FIGURE 9 and FIGURE 10

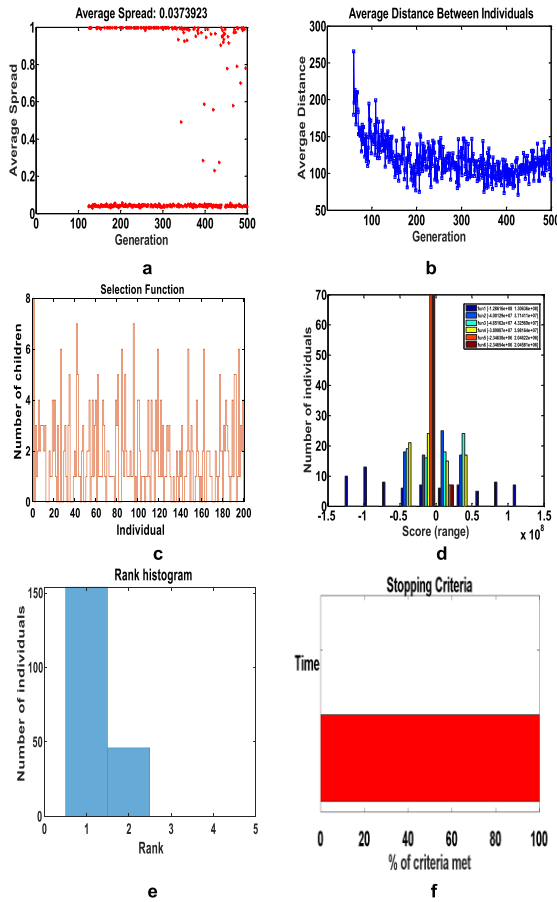


FIGURE 8. (a) Average spread; (b); Average distance between individuals; (c) The selection function; (d) Distance of individuals; (e) Score histogram; (f) Stopping criteria.

shows the optimum joints snap as a function of the robots dynamic model and the constraints defined in (20)-(25). The figures show that the snap variation of the first, second, third, fourth, fifth and sixth joints are smooth, stable, and meet the continuity requirement for snap defined in (20)-(25). The R-SQUARE values for the joints snap shows significant improvement from 0.46, 0.46, 0.46, 0.14, 0.19 and 0.5, for joints shown in FIGURE 9 (a-f) to 0.77, 0.47, 0.69, 0.42, 0.67 and 0.59, for joints shown in FIGURE 10(a-f), with the use of HMOGA (see TABLE 5). This improvement is an indication

TABLE 5. Values of various kinematic parameters after optimisation using MOGA and HMOGA for joint snap.

		Joint 1	Joint 2	Joint 3	Joint 4	Joint 5	Joint 6
Snap( deg s <sup>-4</sup> )							
Nonic Bezier curve+MOGA	Mean	-86.31	-166.1	-61.66	-26.55	-12.19	-50.17
	Max	-69.44	-103.4	-37.86	-24.46	-10.65	-33.90
	R-SQUARE	0.46	0.46	0.46	0.14	0.19	0.50
Nonic Bezier curve+HMOGA	Mean	-56.30	-66.10	-78.13	-47.67	-31.19	-32.91
	Max	-33.10	-55.78	-77.56	-46.22	-21.7	-8.34
	R-SQUARE	0.77	0.47	0.69	0.42	0.67	0.59

TABLE 4. Parameter of the hybrid algorithm.

Population type	Double vector
Population size	200
Creation function	Constrain dependent
Selection function	Tournament
Tournament size	2
Crossover ratio	0.8
Mutation function	Constrain dependent
Crossover function	Constrain dependent
Migration	Both
Migration fraction	0.2
Migration interval	20
The Pareto front population ratio	0.35
Hybrid function	Multi-objective goal attainment
Maximum Generation	500
Stall generation	500
Function tolerance	1e-6
Constrain tolerance	1e-6
Function evaluation	Parallel computing

of how the observed data points fit into the regression model and an indication of the smoothness of the motion.

**B. EFFECT OF THE DEFINED CONSTRAINTS ON THE OPTIMISED JOINT TORQUE**

To validate the effect of the defined constraints on the joint torque, the classical MOGA and the HMOGA optimisation were used. FIGURE 11 and FIGURE 12 shows the results of the variation of the Torques after applying the hybrid optimisation scheme on the welding manipulator. The multi-objective optimisation function is defined and evaluated under the kinematic and dynamic constraints for each link. These dynamic constraints include torque limit at the actuator of each link. The uniqueness of the results of the optimal torques is in the inclusion of the snap constraints (rate of change of jerk) in the objective function. FIGURE 11 and FIGURE 12 shows that the torque variation of the first, second, third, fourth, fifth and sixth joints are smooth, stable, and meet the continuity requirement. The R-SQUARE values for the joints torque show a significant improvement from -0.092, -0.094, -0.10, -0.10, -0.11, -0.11 for joints shown in FIGURE 11(a-f), to 0.57, 0.62, 0.63, 0.62, 0.52 and 0.52, for joints shown in FIGURE 12(a-f) with the use of HMOGA (see TABLE 6). This improvement is an indication of how the observed data points fit into the regression model and the smoothness of the motion.

TABLE 6. Values of various kinematic parameters after optimisation using MOGA and HMOGA for joint torque.

		Joint 1	Joint 2	Joint 3	Joint 4	Joint 5	Joint 6
<b>Optimal Joint Torque (Nm)</b>							
<b>Nonic Bezier curve+MOGA</b>	Mean	-3.19e+6	-1.782e+6	-2.069e+6	1.75e+6	-4.16e+4	-3.89e+4
	Max	1.28e+8	1.691e+7	1.929e+7	9.87e+7	2.23e+6	2.23e+6
	R-SQUARE	-0.092	-0.094	-0.10	-0.10	-0.11	-0.11
<b>Nonic Bezier curve+HMOGA</b>	Mean	-2.4e+11	-1.99e+11	-2.58e+10	1.6e+9	-1.67e+8	-1.3e+8
	Max	1.5e+12	1.8e+9	4.27e+07	2.3e+12	4.71e+9	-3.13e+6
	R-SQUARE	0.57	0.62	0.63	0.62	0.52	0.52

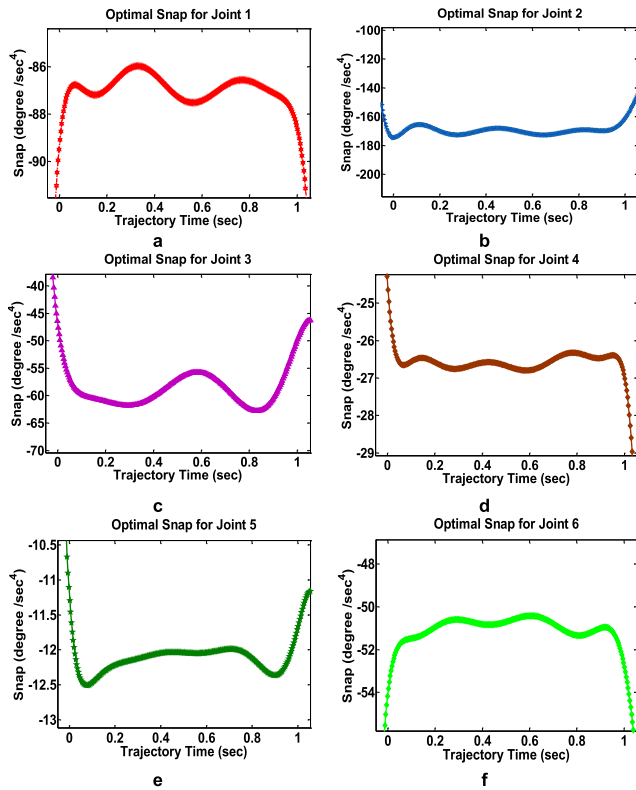


FIGURE 9. Results for designed trajectory along the geometric path using MOGA in terms of the time history of joint snap.

To verify the effect of the defined constraints on the joint angle position, the classical Multi-Objective Genetic Algorithm (MOGA) and the Hybrid Multi-Objective Genetic Algorithm (HMOGA) optimisation were used. The optimised running graphs of each joint angle is plotted in Appendix FIGURE 14 and FIGURE 15. The coefficient of determination, known as R-SQUARE, gives the goodness of fit of the observed data. The figures show that the angle variation of the first, second, third, fourth, fifth and sixth joints are smooth, stable, and meet the continuity requirement for joint angle displacement as defined in (20)-(25). The R-SQUARE values for the joint angles show significant improvement from 0.38, 0.05, 0.19, -0.08, -0.026 and -0.12 for joints shown in FIGURE 14(a-f), to 0.57, 0.711, 0.23, 0.66 and 0.72 shown in FIGURE 15 (a-f), with the use of HMOGA (see TABLE 8). The curve becomes smoother after the use

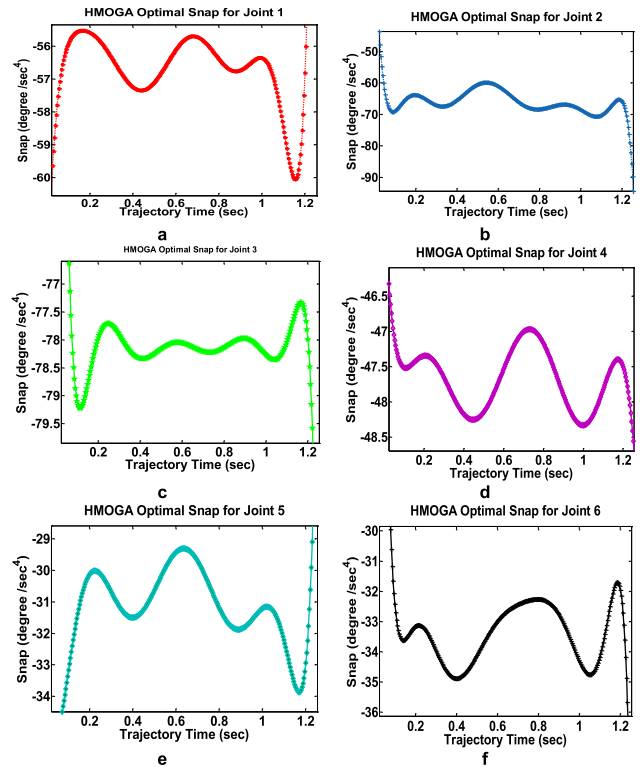


FIGURE 10. Results for designed trajectory along the geometric path using HMOGA in terms of the time history of joint snap.

of HMOGA, and it is an indication of how the displacement data points fit into the regression model; this is seen from the kinematic parameters of the optimal joint displacement shown in Appendix TABLE 8.

To validate the effect of the defined constraints on the joint velocity, the classical MOGA and the HMOGA optimisation were used. FIGURE 16 and FIGURE 17 shows the effects of the defined constraints in (20)-(25), within the framework of the robots dynamic model on the joints velocity. The figures show that the velocity variation of the first, second, third, fourth, fifth and sixth joints are smooth, stable, and meet the continuity requirement for velocity defined in (20)-(25). The R-SQUARE values for the joints velocity shows a significant improvement from 0.09, 0.104, 0.45, 0.43, 0.42 and 0.31 for joints shown in FIGURE 16(a-f) to 0.49, 0.74, 0.70, 0.72, 0.53 and 0.4 for joints shown in FIGURE 17(a-f), with the use of HMOGA (see TABLE 9). This improvement is an indication

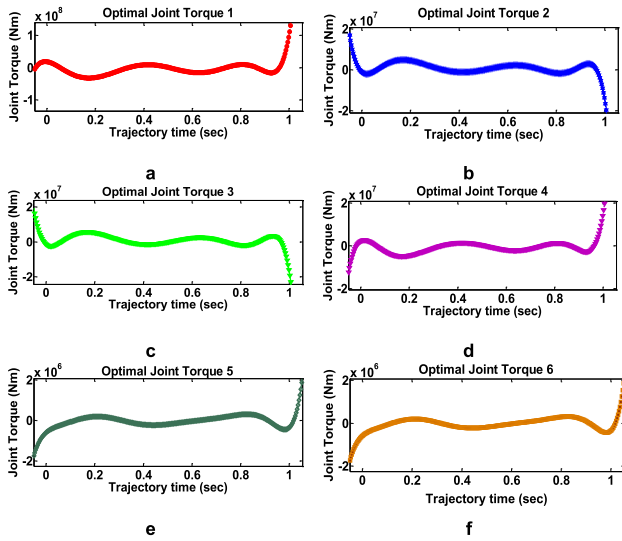


FIGURE 11. Results for designed trajectory along the geometric path using MOGA in terms of the time history of joint torque.

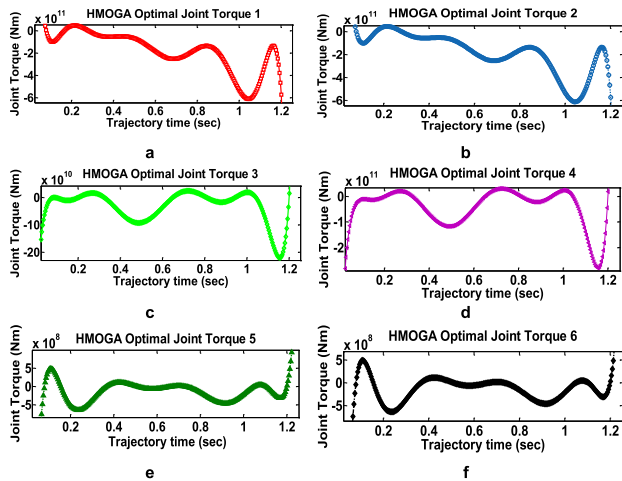


FIGURE 12. Results for designed trajectory along the geometric path using HMOGA in terms of the time history of joint torque.

of how the observed data points fit into the regression model and smoothness of the motion.

To validate the effect of the defined constraints on the joint acceleration, the classical MOGA and the HMOGA optimisation were used. FIGURE 18 and FIGURE 19 shows the minimised joints acceleration as a function of the robots dynamic model and the constraints defined in (20)-(25). The figures show that the acceleration variation of the first, second, third, fourth, fifth and sixth joints are smooth, stable, and meet the continuity requirement for acceleration defined in (20)-(25). The R-SQUARE values for the joints acceleration shows a significant improvement from 0.26, 0.29, -0.01, 0.38, 0.39 and 0.51 for joints shown in FIGURE 18(a-f) to 0.52, 0.53, 0.91, 0.91, 0.77 and 0.49 for joints shown in FIGURE 19(a-f) with the use of HMOGA (see TABLE 10). This improvement is an indication of how the observed data

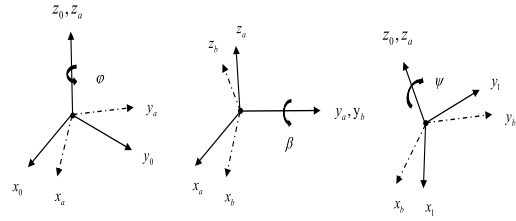


FIGURE 13. Euler angles.

points fit into the regression model and smoothness of the motion. These joints acceleration result is not only seamless but also in agreement with the research work of Jorge [26]; except for the non-inclusion of the jerk and dynamic constraints. Therefore, the results realised the optimal trajectory in terms of the robots dynamic constraints and achieved the expected tracking ability in terms of its optimal joint acceleration.

To confirm the effect of the defined constraints on the joint jerk, the classical MOGA and the HMOGA optimisation were used. FIGURE 20 and VII shows the optimised joints jerk as a function of the robots dynamic model and the constraints defined in (20)-(25). The figures show that the jerk variation of the first, second, third, fourth, fifth and sixth joints are smooth, stable, and meet the continuity requirement for jerk continuity defined in (20)-(25). The R-SQUARE values for the joints jerk shows a significant improvement from 0.50, 0.54, 0.43, 0.37, 0.39 and 0.167 for joints shown in FIGURE 20(a-f) to 0.83, 0.51, 0.71, 0.48, 0.81 and 0.38 for joints shown in FIGURE 21(a-f) with the use of HMOGA (see TABLE 11). This improvement is an indication of how the observed data points fit into the regression model and the smoothness of the motion. These joint jerks results are seamless and incorporate dynamic constraints. Furthermore, the results realised the optimal trajectory in terms of the robots dynamic constraints and achieved the expected tracking ability in terms of its optimal jerk acceleration.

### VII. CONCLUSION

This work demonstrates the use of a hybrid multi-objective optimisation approach for trajectory planning. The objective considered in this work is to carry out the welding task with minimum movement of the joint angles, accelerations, jerks and snap along the weld points keeping in mind the dynamic robot model formulated using the Euler-Lagrangian method and incorporating friction terms. The trajectory design was constructed for all the six joints, using a 9<sup>th</sup> order Bezier curve to accommodate the ten boundary conditions required to satisfy the continuity constraints for joints displacement, velocity, acceleration, jerk and snap. The control point at the initial and final conditions during welding was premised on the assumption that the robot is at rest initially, and comes to a full stop at the end of the trajectory. The scheme combines the multi-objective genetic algorithm and the multi-objective goal attainment algorithm to solve the problem of

TABLE 7. Comparison of results obtained after optimisation.

Optimisation technique	No. of iteration	Trajectory time (sec)	Function count	Average distance	Average spread	Computational time (sec)
MOGA	10,741	1.36	78401	0.0171	0.037	5,567
HMOGA	6,000	1.15	1448471	0.670	0.167	815

TABLE 8. Values of various kinematic parameters after optimisation using MOGA and HMOGA for joint displacement.

		Joint 1	Joint 2	Joint 3	Joint 4	Joint 5	Joint 6
<i>Velocity (deg s<sup>-1</sup>)</i>							
Nonic Bezier curve+MOGA	Mean	-393.60	-216.50	-265.20	-217.40	-169.60	-80.69
	Max	-382.00	-215.40	-262.10	-204.70	-150.10	11.51
	R-SQUARE	0.090	0.1038	0.45	0.43	0.42	0.31
Nonic Bezier curve+HMOGA	Mean	-786.30	-1.1e+4	-1.4e4	-1.2e+4	-5.6e+4	-5.9e+4
	Max	4331	5.5e+4	9695	7.15e+4	258	284
	R-SQUARE	0.49	0.74	0.70	0.72	0.53	0.40

TABLE 9. Values of various kinematic parameters after optimisation using MOGA and HMOGA for joint velocity.

		Joint 1	Joint 2	Joint 3	Joint 4	Joint 5	Joint 6
<i>Velocity (deg s<sup>-1</sup>)</i>							
Nonic Bezier curve+MOGA	Mean	-393.60	-216.50	-265.20	-217.40	-169.60	-80.69
	Max	-382.00	-215.40	-262.10	-204.70	-150.10	11.51
	R-SQUARE	0.090	0.1038	0.45	0.43	0.42	0.31
Nonic Bezier curve+HMOGA	Mean	-786.30	-1.1e+4	-1.4e4	-1.2e+4	-5.6e+4	-5.9e+4
	Max	4331	5.5e+4	9695	7.15e+4	258	284
	R-SQUARE	0.49	0.74	0.70	0.72	0.53	0.40

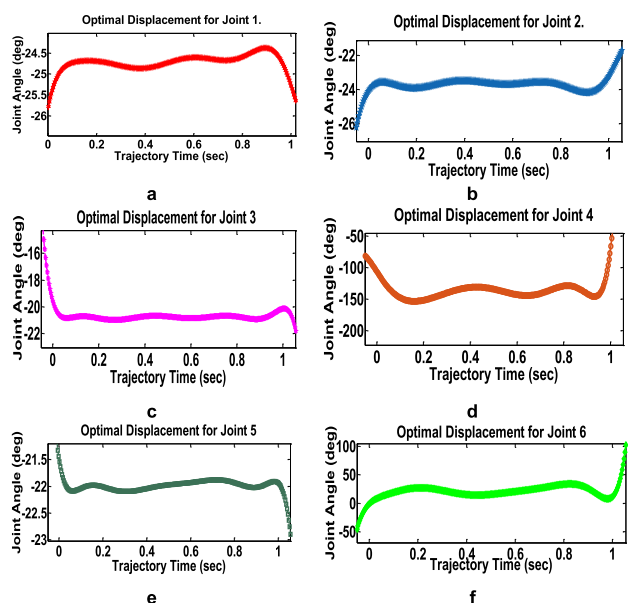


FIGURE 14. Results for designed trajectory along the geometric path using MOGA in terms of the time history of Joint displacement.

the total tracking error reduction during arc welding. After designing the trajectory optimisation function for all the constraints using the nonic Bezier curve, the optimisation was carried out using MOGA and HMOGA. Global optimum

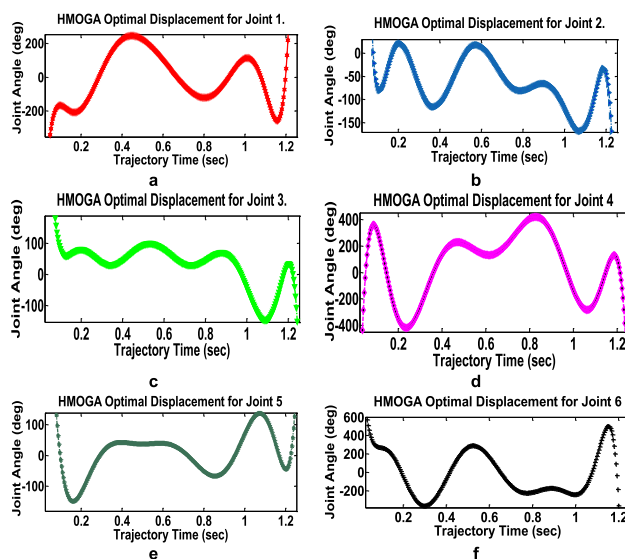


FIGURE 15. Results for designed trajectory along the geometric path using HMOGA in terms of the time history of Joint displacement.

solutions using HMOGA are compared and analysed with that of MOGA. It was that HMOGA gives better results than MOGA (see TABLE 7). Also, HMOGA converges faster than MOGA. The ensuing optimised trajectories from HMOGA and MOGA have DVAJS within their bounds and only need minimal actuator effort. The mean and maximum

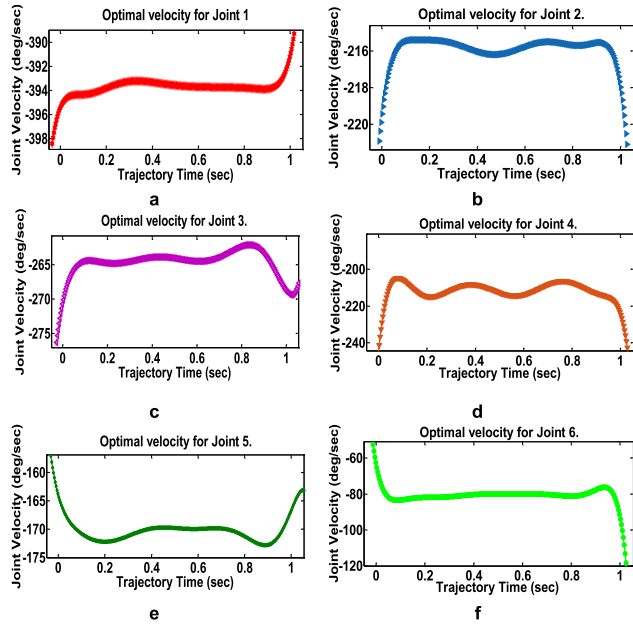


FIGURE 16. Results for designed trajectory along the geometric path using MOGA in terms of the time history of joint velocity.

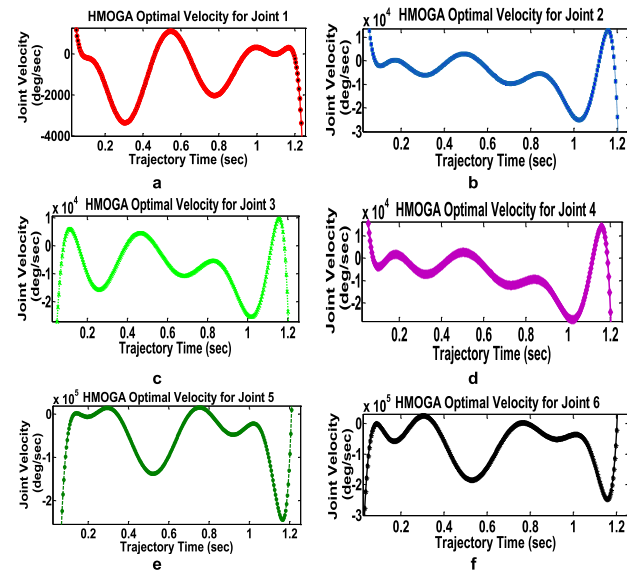


FIGURE 17. Results for designed trajectory along the geometric path using HMOGA in terms of the time history of joint velocity.

values of the kinematic parameters obtained using MOGA and HMOGA are shown in TABLE 5-TABLE 6 and also Appendix TABLE 8 to TABLE 11. The values of these parameters are within the kinematic constraints imposed on the manipulator. A summary of key performance indicators from a comparison of results obtained after optimisation is shown in TABLE 7. The use of HMOGA shows an improved average spread, average distance, number of iteration and computational time. It can be concluded that from the constraints studied, the optimal path in terms of the robot's dynamic

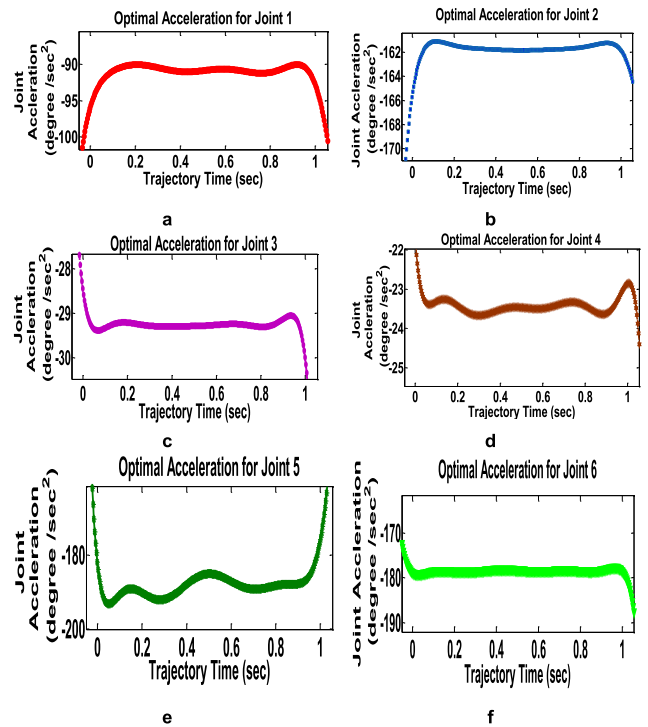


FIGURE 18. Results for designed trajectory along the geometric path using MOGA in terms of the time history of joint acceleration.

constraints can achieve the expected tracking ability in terms of the optimal DVAJS.

## APPENDIX

### A. EULER ANGLES Z-Y-Z CONVENTION

The Euler angle conventions used to describe orientation are Z-X-Z, X-Y-X, Y-Z-Y, Z-Y-Z, X-Z-X, and Y-X-Y. The Euler angle transformation used in this work is the Z-Y-Z convention (see FIGURE 13).

The Z – Y – Z Euler angle transformation is shown in (26), as shown at the bottom of the next page.

The Euler angles represent three rotations relative to the three major axes of the coordinate frame. They are denoted as Roll  $\varphi$  for  $x$  – axis rotation, Pitch  $\beta$  for  $y$  – axis rotation and Yaw  $\psi$  for  $z$  – axis.

The sequel shows the solution for extracting Z – Y – Z Euler angles. Given

$$R_{z,\varphi}R_{y,\beta}R_{z,\psi} = \begin{bmatrix} r_{11} & r_{12} & r_{13} \\ r_{21} & r_{22} & r_{23} \\ r_{31} & r_{32} & r_{33} \end{bmatrix}, \quad (27)$$

Then if  $\sin \beta \neq 0$ , it follows that

$$\begin{aligned} \beta &= \arctan 2 \left( \sqrt{r_{31}^2 + r_{32}^2}, r_{33} \right), \\ \varphi &= \arctan 2 \left( r_{23}/\sin \beta, r_{13}/\sin \beta \right), \\ \psi &= \arctan 2 \left( r_{32}/\sin \beta, -r_{31}/\sin \beta \right). \end{aligned} \quad (28)$$

### B. EFFECT OF THE DEFINED CONSTRAINTS ON THE JOINT ANGLE POSITION

See Figures 14, 15, and Table 8.

**TABLE 10.** Values of various kinematic parameters after optimisation using MOGA and HMOGA for joint acceleration.

		Joint 1	Joint 2	Joint 3	Joint 4	Joint 5	Joint 6
Acceleration (deg s <sup>-2</sup> )							
Nonic Bezier curve+MOGA	Mean	-91.61	-162.20	-29.29	-23.17	-185.40	-177.90
	Max	-90.04	-161.10	-24.36	-13.28	-115.10	-163.00
	R-SQUARE	0.26	0.29	-0.01	0.38	0.39	0.51
Nonic Bezier curve+HMOGA	Mean	-3.76e+05	-2.87e+5	-2.87e+05	-2.86e+5	-1.94e+5	-13.26
	Max	1.41e+07	4.23e+4	4.2e+04	4.27e+4	178	107.10
	R-SQUARE	0.52	0.53	0.91	0.91	0.77	0.49

**TABLE 11.** Values of various kinematic parameters after optimisation using MOGA and HMOGA for joint jerk.

		Joint 1	Joint 2	Joint 3	Joint 4	Joint 5	Joint 6
Jerk (deg s <sup>-3</sup> )							
Nonic Bezier curve+MOGA	Mean	-67.64	-32.38	-52.44	-120.9	-32.75	-5.268
	Max	-50.25	-27.59	-31.91	-117.4	-10.91	-4.322
	R-SQUARE	0.50	0.54	0.43	0.37	0.39	0.167
Nonic Bezier curve+HMOGA	Mean	-53.32	-71.53	-54.96	-131.6	-37.96	-12.96
	Max	-45.19	-70.99	-37.91	-128.9	-36.89	-11.04
	R-SQUARE	0.83	0.51	0.711	0.48	0.81	0.38

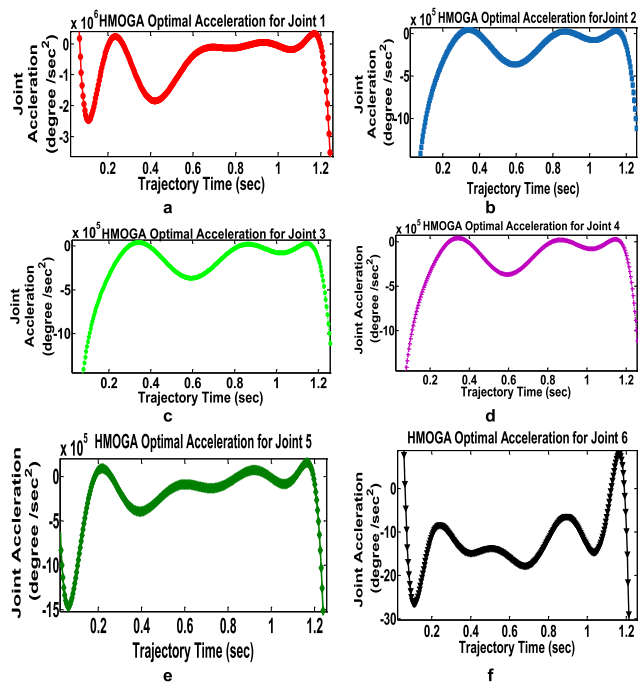


**FIGURE 19.** Results for designed trajectory along the geometric path using HMOGA in terms of the time history of joint acceleration.

**C. EFFECT OF THE DEFINED CONSTRAINTS ON THE OPTIMISED JOINT VELOCITIES**

See Figures 16, 17, and Table 9.

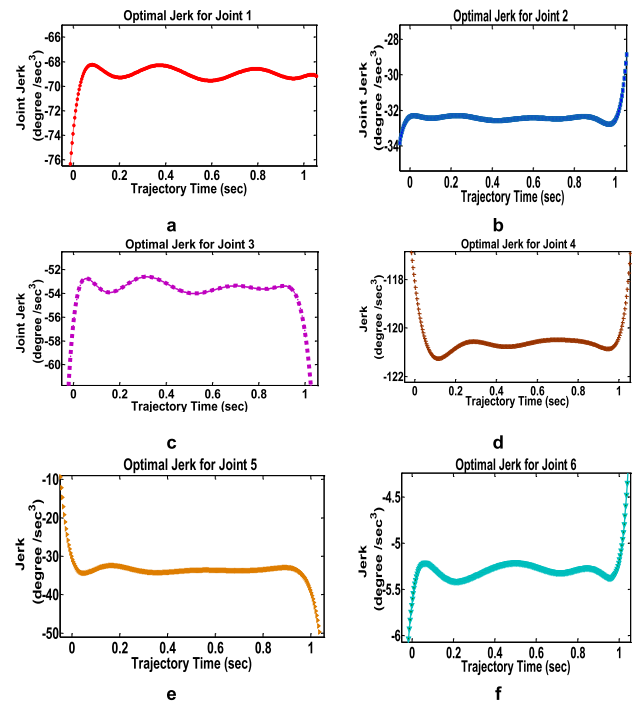


**FIGURE 20.** Results for designed trajectory along the geometric path using MOGA in terms of the time history of joint jerk.

**D. EFFECT OF THE DEFINED CONSTRAINTS ON THE OPTIMISED JOINT ACCELERATION**

See Figures 18, 19, and Table 10.

$$R_{ZYZ} = R_{z,\varphi}R_{y,\beta}R_{z,\psi} = \begin{bmatrix} \cos \varphi \cos \beta \cos \psi - \sin \varphi \sin \psi & -\cos \varphi \cos \beta \sin \psi - \sin \varphi \cos \psi & \cos \varphi \sin \beta \\ \sin \varphi \cos \beta \cos \psi + \cos \varphi \sin \psi & -\sin \varphi \cos \beta \sin \psi + \cos \varphi \cos \psi & \sin \varphi \sin \beta \\ -\sin \varphi \cos \psi & \sin \varphi \sin \psi & \cos \beta \end{bmatrix} \quad (26)$$

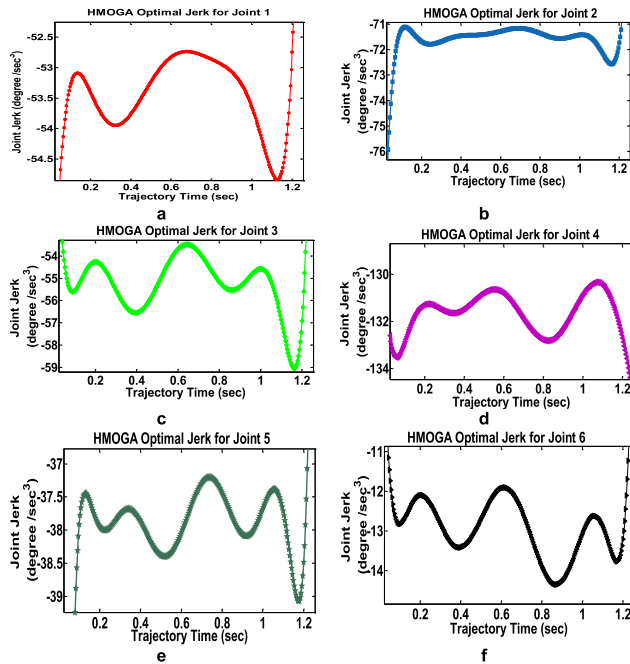


**FIGURE 21.** Results for designed trajectory along the geometric path using HMOGA in terms of the time history of joint jerk.

**E. EFFECT OF THE DEFINED CONSTRAINTS ON THE OPTIMISED JOINT JERK**

See Figures 20, 21, and Table 11.

**ACKNOWLEDGEMENT**

The authors are very grateful to the following; Gibela Rail Transport Consortium, Innovative Manufacturing and Design Solution (IMDS) Group and the Tshwane University of Technology (TUT) for providing relentless support during the research. Special thanks to Dr A. J Onumanyi, Dr O.M Olanbaji and Dr B.I Ramatsetse for assisting in critiquing this article.

**REFERENCES**

[1] Railway Gazette. (Oct. 2015). *First South West Trains Class 707 EMU Under Construction*. Railway Gazette. [Online]. Available: <https://www.railwaygazette.com/>

[2] Vedsasso. (2017). *Bogie Frame Assembly for Locomotives and Coaches*. [Online]. Available: <http://vedsassos.com/products.html>

[3] J. Ogbemhe, K. Mpofu, N. Tlale, and B. Ramatsetse, "Application of robotics in rail car manufacturing learning factory: A case of welding complex joints," *Proc. Manuf.*, vol. 31, no. 1, pp. 316–322, 2019.

[4] A. Owen-Hill, "How to benefits from robotic shortage," in *Robotics Industry News, Applications and Trends*, vol. 2016. Lévis, QC, Canada: Robotiq Company, 2016.

[5] J. Ogbemhe and K. Mpofu, "Towards achieving a fully intelligent robotic arc welding: A review," *Ind. Robot.*, vol. 42, no. 5, pp. 475–484, 2015.

[6] J. Ogbemhe, K. Mpofu, and N. S. Tlale, "Continuous trajectory planning for welding of complex joints using Bezier curve," *Proc. Manuf.*, vol. 33, no. 1, pp. 685–692, 2019.

[7] J. Ogbemhe, K. Mpofu, and N. S. Tlale, "Achieving sustainability in manufacturing using robotic methodologies," *Proc. Manuf.*, vol. 8, no. 1, pp. 440–446, 2017.

[8] S. S. Chiddarwar and N. R. Babu, "Optimal trajectory planning for industrial robot along a specified path with payload constraint using trigonometric splines," *Int. J. Automat. Control*, vol. 6, no. 1, pp. 39–65, 2012.

[9] A. Gasparetto, P. Boscaroli, A. Lanzutti, and R. Vidoni, "Trajectory planning in robotics," *Math. Comput. Sci.*, vol. 6, no. 3, pp. 269–279, 2012.

[10] J. N. Pires, E. J. Lima, and A. Q. Bracarense, "Trajectory generation in robotic shielded metal arc welding during execution time," *Ind. Robot.*, vol. 36, no. 1, pp. 19–26, 2009.

[11] J. Mattmüller and D. Gisler, "Calculating a near time-optimal jerk-constrained trajectory along a specified smooth path," *Int. J. Adv. Manuf. Technol.*, vol. 45, nos. 9–10, p. 1007, 2009.

[12] F. Jing, Y. Qi, Y. Qiang, and C. Yang, "An on-line robot trajectory planning algorithm in joint space with continuous accelerations," in *Proc. Int. Conf. Adv. Technol. Design Manuf. (ATDM)*, 2010, pp. 372–377.

[13] Y. Chen and B. Li, "A piecewise acceleration-optimal and smooth-jerk trajectory planning method for robot manipulator along a predefined path," *Int. J. Adv. Robotic Syst.*, vol. 8, no. 4, p. 50, 2011.

[14] F. Rubio, F. Valero, J. Sunyer, and J. Cuadrado, "Optimal time trajectories for industrial robots with torque, power, jerk and energy consumed constraints," *Ind. Robot.*, vol. 39, no. 1, pp. 92–100, 2012.

[15] P. Freeman, "Minimum jerk trajectory planning for trajectory constrained redundant robots," Ph.D. dissertation, Dept. Elect. Syst. Eng., Washington Univ. St. Louis, St. Louis, MO, USA, 2012.

[16] Z. Liu, W. Bu, and J. Tan, "Motion navigation for arc welding robots based on feature mapping in a simulation environment," *Robot. Comput.-Integr. Manuf.*, vol. 26, no. 2, pp. 137–144, 2010.

[17] C. Chen, S. Hu, D. He, and J. Shen, "An approach to the path planning of tube-sphere intersection welds with the robot dedicated to J-groove joints," *Robot. Comput.-Integr. Manuf.*, vol. 29, no. 4, pp. 41–48, 2013.

[18] Z. Dai, X. Sheng, J. Hu, H. Wang, and D. Zhang, "Design and implementation of Bézier curve trajectory planning in DELTA parallel robots," in *Proc. Int. Conf. Intell. Robot. Appl.* Shanghai, China: Shanghai Jiao Tong Univ., School of Mechanical Engineering, 2015, pp. 420–430.

[19] Z. Duan and X. Meng, "Welding trajectory planning of beam welding robot based on computer simulation," in *Proc. 2nd Int. Conf. Elect., Comput. Eng. Electron.*, vol. 2, no. 1. Paris, France: Atlantis Press, Jun. 2015.

[20] T. T. Su, L. Cheng, Y. K. Wang, X. Liang, J. Zheng, and H. Zhang, "Time-optimal trajectory planning for delta robot based on quintic pythagorean-hodograph curves," *IEEE Access*, vol. 6, pp. 28530–28539, 2018.

[21] A. Reiter, A. Müller, and H. Gatringer, "On higher order inverse kinematics methods in time-optimal trajectory planning for kinematically redundant manipulators," *IEEE Trans. Ind. Informat.*, vol. 14, no. 4, pp. 1681–1690, Apr. 2018.

[22] P. Shen, X. Zhang, and Y. Fang, "Complete and time-optimal path-constrained trajectory planning with torque and velocity constraints: Theory and applications," *IEEE/ASME Trans. Mechatronics*, vol. 23, no. 2, pp. 735–746, Apr. 2018.

[23] L. Biagiotti and C. Melchiorri, *Trajectory Planning for Automatic Machines and Robots*. Berlin, Germany: Springer-Verlag, 2008.

[24] *KR QUANTEC extra HA Specification*, KUKA, Augsburg, Germany, 2018.

[25] A. A. Ata, "Optimal trajectory planning of manipulators: A review," *J. Eng. Sci. Technol.*, vol. 2, no. 1, pp. 32–54, 2007.

[26] A. Jorge, *Fundamentals of Robotic Mechanical Systems: Theory, Methods, and Algorithms*, F. F. Ling, Ed. 4th ed. Cham, Switzerland: Springer, 2014.



**JOHN OGBEMHE** received the B.Eng. degree in agricultural engineering (Second class upper division) from the Federal University of Technology Akure (FUTA), Nigeria, in 2003, and the M.Sc. degree (Hons.) in systems engineering (artificial intelligence option) from the University of Lagos, Nigeria. He is currently pursuing the Ph.D. degree with the Tshwane University of Technology (TUT), South Africa. He is also a Lecturer with the Department of Systems Engineering, University of Lagos (UNILAG). His research focuses on industrial robotics, digital manufacturing, and ROS-I applications to advance manufacturing. He is currently a member of the South African Institute of Industrial Engineering (SAIIE), a member of the Nigerian Society of Engineers (NSE), and a certified and registered engineer with the Council for the Regulation of Engineering in Nigeria (COREN). He is a member of the CIRP Design 2020 Administration Team, and has scholarly works with reputable journals and conferences. He has reviewed papers for various conferences.



**KHUMBULANI MPOFU** is currently a Professor of industrial engineering and the Gibela Research Chair in Manufacturing and Skills Development with the Tshwane University of Technology (TUT), South Africa. He is an NRF-rated researcher with an unbridled passion for industrial engineering. He has reviewed papers for various conferences, including the CIRP Conference on Manufacturing Systems, the CIRP Global Conference on Sustainable Manufacturing, the Flexible

Automation and Intelligent Manufacturing Conference, the Southern African Institute of Industrial Engineers Conference, the Zimbabwe Institute of Engineers, the International Conference on Appropriate Technology, the Symposium on Mechatronics and Robotics, the Botswana Institute of Engineers Conference, the Conference on Mechatronics and Machine Vision, Hybrid and Intelligent Systems, the International Federation of Automatic Control Conference, and the CIRP Global Conference on Manufacturing. In 2008, he chaired the much-acclaimed session at the International Conference on CAD/CAM and Robotics and Factories of the Future. He has also participated in the CIRP General Assembly Local Organizing Committee held in Cape Town, South Africa, in 2015. He currently serves the CIRP Global Conference on Sustainable Manufacturing and is the Conference Chair for the 30th CIRP Design Conference.



**NKGATHO TLALE** received the B.Sc. (Mech.) Eng., M.Sc. (Eng.), and Ph.D. degrees from the University of KwaZulu Natal (UKZN), and the MBA degree from the University of Pretoria. He is currently an Executive Manager for Systems and Automation, Transnet Engineering, South Africa. He is currently an extraordinary Professor with the Department of Industrial Engineering, Tshwane University of Technology (TUT), South Africa. He is also a Mechatronics and Advanced Manufac-

turing Engineer with many years of experience in mining and transportation. He is an active participant in South African operations and in the development of new business in the Southern African region. Upon completing his B.Sc. (mechanical engineering) at UKZN, he has published extensively in the fields of advanced manufacturing, mechatronics, and robotics. He is a former Research Group Leader at the Council for Scientific and Industrial Research (CSIR), South Africa. Before joining CSIR, he held several academic positions at Massey University, New Zealand, and the University of Pretoria, South Africa, respectively. In these roles, he conducted research and taught several courses in advanced manufacturing, mechatronics, and robotics. His current research interests are AMR, parallel kinematics manipulators, and RMS.

• • •